JMATPRO	Journal of Advanced Materials and Processing 11 (2): 15-29, Spring 2023 http://jmatpro.iaun.iau.ir

Research Paper

Evaluation of Flow Behavior of Novel Titanium Ti-3873 Alloy Via Compressive Deformation in Two Phase α/β and Single Phase β Regions

Mahnaz Dabaghi [1], Maryam Morakabati[2*]

1. MS. C., Faculty of Materials and Manufacturing Technologies, Malek Ashtar University of Technology, Tehran, Iran.

2. Associate Professor, Faculty of Materials and Manufacturing Technologies, Malek Ashtar University of Technology, Tehran, Iran.

ARTICLE INFO

Article history:

Received 26 December 2023
Accepted 09 June 2024
Available online 1 May 2023

Keywords:
Ti-3Al-8Mo-7V-3Cr alloy
arm compression test
recovery
recrystallization
activation energy
processing map

ABSTRACT

Semi-stable β-titanium (Ti-3873) Ti-3Al-8Mo-7V-3Cr alloy with excellent workability properties has been designed based on high demanded aircraft Ti-5Al-5Mo-5V-3Cr alloy according to semi-experimental d-electron approach. The aim of the present research is to investigate the deformation behavior of Ti-3873 alloy via warm compression test. For this purpose, compression test has been conducted in the temperature range of 650-850 °C and strain rates of 0.001,0.1 and 1, 1 s^{-1} at dual phase α/β and single phase β regions. The test was continued up to plastic strain of 0.7. For establishing the relationship between the microstructure and flow behavior, the initial and subsequent microstructure of the specimens after warm deformation was studied via optical and scanning electron microscopes. The microstructural evaluation and flow curves revealed that dynamic recovery and partial continuous dynamic recrystallization were the dominant restoration mechanisms. The results showed that softening has been increased in the temperature range of 800-850 °C and strain of 0.001 and 0.1 s^{-1} which is confirmed by the activation energy calculated from the sinus hyperbolic equation. The activation energy for dual phase α/β and single phase β regions are determines as 429 kJ/mol and 353 kJ/mol, respectively. The higher value of activation energy for α/β dual phase region is attributed to dynamic globularization of α lamellas. The preferable regions for hot workability of the alloy were achieved at the temperature range of 800-850 °C and strain rate of 0.01-0.001 s^{-1} corresponding to the peak efficiency of 39% in the processing map.

Citation: Dabaghi, M.; Morakabati, M. (2023). Evaluation of Flow Behavior of Novel Titanium Ti-3873 Alloy Via Compressive Deformation in Two Phase α/β and Single Phase β Regions, Journal of Advanced Materials and Processing, 11 (2), 15-29.

[*] **Corresponding Author:**
E-Mail: m_morakabati@mut.ac.ir

1. Introduction

In recent decades, a novel method named as molecular orbital calculations has been developed to develop special alloys. The relationship between the phase stability, physical and mechanical properties has been established using this approach [1-3]. By manipulating this method, it is practical to developed the special alloys such as twining induced transformation alloys [4-5]. This technique was introduced in order to design a novel β-Ti alloy with appropriate properties for orthopedic or aerospace applications [6-9]. Ti-5Al-5Mo-5V-3Cr (Ti-5553) is a commercial β-titanium alloy with wide applications in aerospace industry [10]. This alloy and its various grades were the research topics in different branches including phase transformation, high temperature mechanical properties and warm deformation behavior [11]. Recently, new studies based on molecular orbitals calculations were fulfilled. As a result of this studies, the Ti-3Al-8Mo-7V-3Cr (Ti-3873) alloy has been introduced as an appropriate alternative for Ti-5553 alloy which shows better strength and formability at room temperature [12, 13]. In this approach, two parameters including energy level of orbital d (Md) and bonding degree (Bo) was derived and subsequently $\overline{Bo} - \overline{Md}$ diagram of the β-titanium alloys was illustrated. In this diagram, Md parameter is referring to the electronegativity and atomic radius of the alloy element and Bo parameter describes the strength of covalence bonding between titanium and other alloying elements. According to the diagram presented in Fig. 1, β-phase stability of each alloy is determined and the deformation mechanism of it is studied. Generally, increasing in β-phase stability leads to an increase in the Mo equivalent value and then decrease the Md and Bo parameters. In Fig. 1, it was clearly observed that by increasing the Bo parameter and decreasing Mo parameter, the deformation mechanism of the alloy is changed from the stress induced martensite transformation to slip and twining. In this alloy the cross slipping and twining is slightly active. By calculating the Mo equivalent parameter and the number of the valance electrons it can be declared that the β-phase of Ti-3873 alloy is more stable than that of the Ti-5553 alloy.

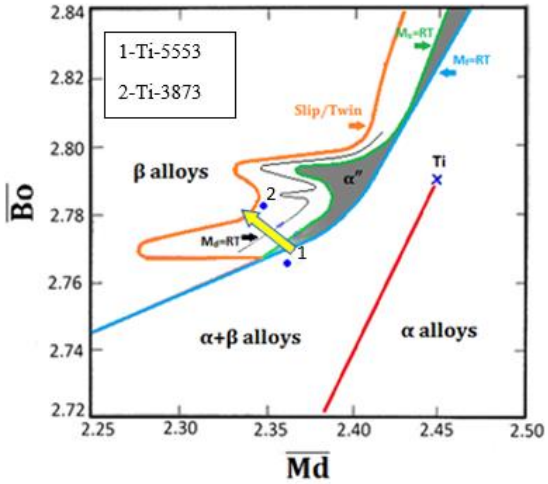

Fig. 1. Deformation mechanism range for the designed titanium alloys in $\overline{\mathbf{Md}}$–$\overline{\mathbf{Bo}}$ diagram [7].

In addition, it was reported that the bonding strength of the Ti-3873 alloy is higher than that of Ti-5553 alloy which is related to its higher stability of β-phase and higher Mo equivalent parameter. Therefore, this alloy has high workability [14]. In Fig. 1, the positions of reference alloy (i.e., Ti-5553) and the designed alloy (i.e., Ti-5873) in $\overline{Md}$–$\overline{Bo}$ diagram are exhibited. However, lack of sufficient information in the case of high temperature application of the Ti-3873 alloy cause postponing in substituting of this alloy with the Ti-5553 alloy. Previous researches [15-17] revealed that dynamic recovery (DRV) and dynamic recrystallisation (DRX) control the microstructure and mechanical behavior of the β-titanium alloys. The volume fraction of recrystallized grains is related to the stacking fault energy (SFE). As known, SFE is a function of the chemical composition. Therefore, it is expected that by changing the chemical composition of the Ti-5553 alloy and the development of the Ti-3873 alloy, the formability of the novel alloy will be changed. Therefore, optimizing the deformation condition of the novel alloy is needed.

The microstructure and mechanical behavior of the semi-stable β-titanium alloy is usually sensitive to the deformation parameters. During the deformation, recovery and recrystallisation has been extensively occurred leading to achieve excellent mechanical

properties. For instance, Momeni et al [18], studied the hot compression behavior of the Ti-5553 alloy at the temperature range of 930-1080 °C and strain rate of 0.001-1 sec-1. The result revealed that the flow behavior of the alloy was predominantly controlled by dynamic recovery and continuous dynamic recrystallisation at temperature of 1080 °C and strain rate of 0.001 sec-1. Other researchers [19] investigated the hot deformation behavior of the Ti-22Al-25Nb alloy by developing the processing map. It has been reported that the main mechanism of the hot deformation of the alloy is the globularization of the initial α grains. Zhu et al. [20] analyzed the flow behavior of the SP-700 alloy by developing the processing map. They evaluate the unstable regions of the map, as well.

The main aim of the present research is to investigate the warm deformation behavior of the Ti-3873 alloy. The restoration mechanism and activation energy of the deformation at dual phase α/β and single phase β regions have been determined. For this purpose, the compression test has been carried out at different temperatures and strain rates. The flow curves have been predicted using constitutive equations. Consequently, the processing map of the alloy has been developed in order to determine the stable regions during deformation. Subsequently, regarding the power dissipation energy of the processing map, the deformation condition of the Ti-3873 alloy was optimized.

2. Materials and experimental investigation

The studied alloy was manufactured 2 times to ensure chemical homogeneity via melting and remelting process in vacuum arc remelting (VAR) furnace. The first stage includes melting the briquettes of granules of titanium sponge with appropriate alloy-containing material. The second stage is remelting the electrode produced from the previous stage. It should be noted that the ingot was prepared by melting pure elements. In order to obtain homogenous microstructure, the homogenization heat treatment had been carried out at the temperature of 1000 °C for 5 hours. Then the ingot was immediately hot rolled at the same temperature. The reduction in thickness during rolling was approximately 60 %. The chemical composition of the alloy was analyzed using scanning electron microscopy (TESCAN) equipped the EDS detector. The nominal composition of the alloy is summarized in table 1. It was clearly observed that the chemical composition of the Ti-3873 alloy is in accordance with its nominal composition.

Table 1. The EDS analysis of the Ti-3873 alloy.

Element	Cr	V	Mo	Al	Ti
Nominal composition	3	7	8	3	79
Chemical Analysis	2.8	7.1	7.8	3.1	79.2

The content of oxygen, nitrogen and hydrogen has been measured by gas analyzer method using Leco-TCH600 machine. The results are reported in table 2.

Table 2. The result of gas analyzer for Ti-3873 alloy (ppm).

Element	N	H	O
Gas analyzer of the specimen	<1	<1	2150

The β-transus temperature of the alloy was determined using metallographic technique in the range of 740-800 °C. According to this method, the Tβ of the alloy was recorded to be 750 ± 10 °C. In order to investigate the effect of temperature and strain rate on the compressive deformation of the Ti-3873 alloy, cylindrical compression specimens with 8 mm in diameter and 12 mm in height were prepared according to the ASTM E209 standard. The graphite powder was used as lubricant. The uniaxial compression test has been carried out at the temperature of the 650, 700, 750, 800 and 850 °C and strain rates of 0.001, 0.1 and 1 s^{-1}. Then specimens rapidly quenched in water. The specimens were preheated for 10 minutes at the temperature of warm compression test. The tests were performed using an Instron 8502 machine equipped with furnace. Prior to compression test, the specimens were homogenized at the single phase β region at 830 °C for 30 minutes. The microstructure of the specimen after homogenization can be observed in Fig. 2. As seen, the microstructure contains the equiaxed grains with mean grain size of 70 µm. To reveal the deformed microstructures, prepared specimens were etched with Kroll's reagent (2 ml HF, 6 ml HNO3, 92 ml H2O).

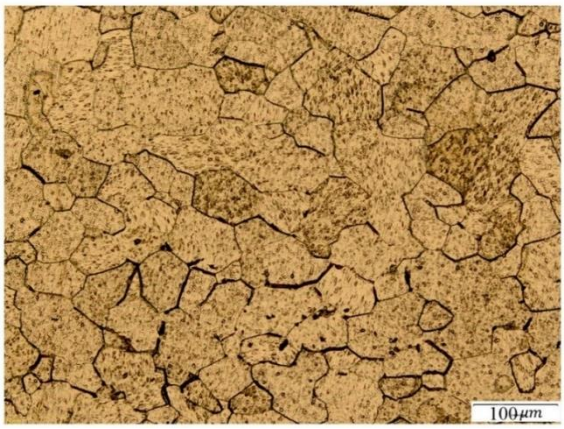

Fig. 2. The microstructure of the Ti-3873 alloy after annealing at 830 °C for 30 minutes.

The relationship between head velocity (V) and strain rate ($\dot{\varepsilon}$) during compression test was derived as the following equation (Eq. 1.):

$$\dot{\varepsilon} = \frac{V}{L_0} \quad (1)$$

where, L0 is referred to the initial height of the specimen. During the compression test, height reduction of the specimen leads to variation in strain rate. Decreasing in height of specimen resulted in gradually increasing the strain rate value. Therefore, for remaining constant strain rate value, the head velocity is continuously decreased. Hence, in this condition the ratio of V/L0 keeps unchanged. The strain distribution and temperature gradient via compression test has been simulated using Deform software.

2.1 The Correction of flow curves for heat of deformation

Deformation heating may also result in a temperature increase in an 'isothermal' test which leads to flow softening. While sufficient time for dissipation of heat at low strain rates allows deformation to progress isothermally, at higher strain rates the entrapment of deformation heat results in adiabatic heating of specimen. This feature suggests that further factors such as heat transfer constants of the material affect the temperature rise. The materials possessing low heat capacity, low thermal conductivity, and high strength are more sensitive to temperature rise impeding heat transfer to outside. In this work, the effect of heat of deformation on flow stress was calculated. At first step, for each strain and strain rate, the stress level at deformation temperature was extracted and the function of $\sigma = f(T)|_{\varepsilon,\dot{\varepsilon}}$ was derived. Form the variation of temperature (ΔT), the variation of the stress ($\Delta\sigma$) obtained as the following equation (Eq. 2) [21]:

$$\Delta\sigma = \Delta T \left.\frac{d\sigma}{dT}\right|_{\varepsilon,\dot{\varepsilon}} \quad (2)$$

After calculating the stress variation, the computed value has been added to the stress obtained from the compression test and the adiabatic heating effect was corrected in the flow curves.

2.2. The Correction of flow curves for friction

By increasing the applied strain, the contact between the surface of the specimen and mandrel is increased resulted in higher value of friction. Therefore, the required driving force for the deformation process is increased and the deformation becomes heterogenous. Hence, the stress level in this condition is higher than the friction free condition. Increase in the stress level is directly related to the friction coefficient of the material ($m_f = \frac{\tau}{k}$); where, τ and k are referred to the shear stress and yield stress, respectively. Consequently, the derived flow curves without friction corrections does not introduce the flow behavior of the material. The flow behavior was corrected for friction using the Ivanz- Sharning relation (Eq. 3) [22]:

$$\sigma = \sigma_{meas}\left(1 + \frac{2}{3\sqrt{3}} m_f \frac{r_0}{h_0}\exp\left(\frac{3\varepsilon}{2}\right)\right)^{-1} \quad (3)$$

where, ro = initial radius (mm), ho= initial height (mm), mf= friction coefficient, σ= corrected flow stress (MPa).

3. Results and Discussion

3.1. Flow stress behavior of the Ti-3873 alloy

The flow curves of the Ti-3873 alloy in dual phase α/β region and single phase β region have been presented in Fig. 3.a and 3.b, respectively. In this figure, only the result of deformation at temperatures of 650 and 850 °C and the applied strain rate of 0.001, 0.1 and 1 s^{-1} are represented.

As it is seen, at a given temperature, the flow stress increases with increasing strain rate. Two types of stress strain curves are presented in the figure: one type is characterized by a "peak stress" where the true stress is reached to maximum and then it is decreased with increase in strain (Fig. 3.a) . While, the second type is characterized by a "steady state stress" in which the stress remained essentially constant from initial yielding to the maximum strain (Fig. 3.b). As it is known, the first one is related to deformation in

dual phase α/β region and the second one is related to deformation in single phase β region. It was clearly observed that the drastically drop in the curves is related to the highest value of the strain rate (i.e., $\dot{\varepsilon} = 1s^{-1}$). The main reason for this behavior is attributed to the adiabatic heating, the microstructural evolution, phase transformation and the propagation of micro-cracks via deformation [23]. The flow stress drop at the higher strain rates and lower temperatures are noticeably high.

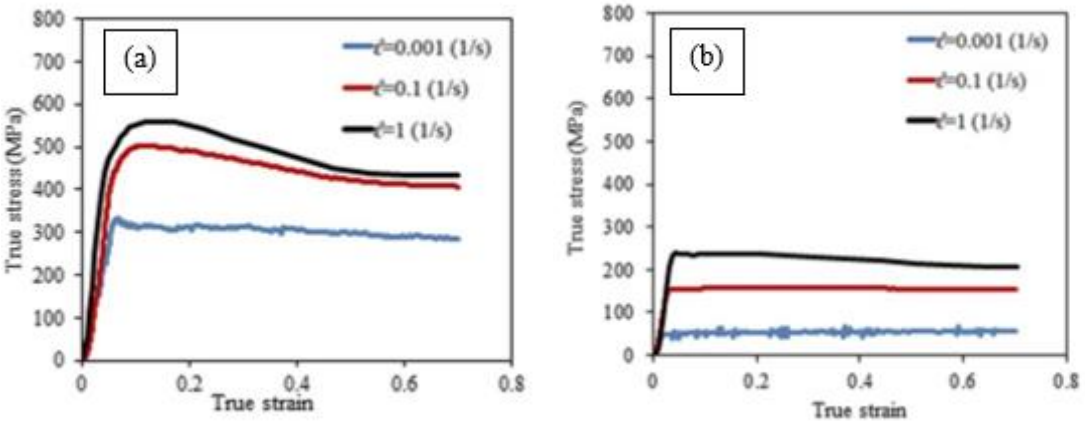

Fig. 3. The stress-strain curves of the Ti3873 alloy at strain rates of 0.001, 0.1 and 1 s^{-1} and temperatures of a) 650 °C, b) 850 °C.

Adiabatic heating leads to non-uniform deformation resulted to the shear band formation at low temperature and high strain rate. In Fig. 4, the appearance of shear bands at the temperature of 650 and 700 °C and strain rate of 1 s^{-1} is shown. According to this figure, it can be deduced that instability mechanism in this region is predominantly related to the localization of deformation. The orientation between the shear bands and the applied stress which is formed at the temperature of 650 and 700 °C is about 45°. This phenomenon is attributed to the generation of heat at high strain rates. Low thermal conductivity of the titanium alloys in comparison with other metallic materials (like Aluminum and steel) is another important parameter facilitating the localization of deformation at this alloy.

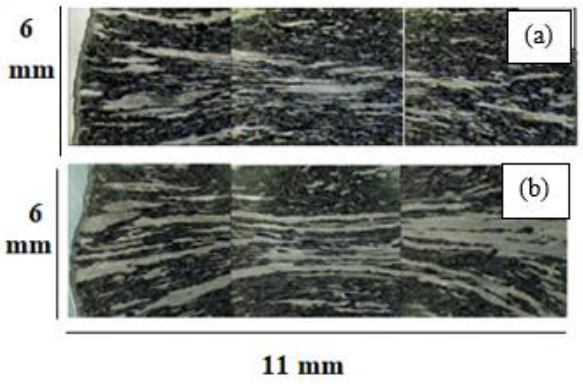

Fig. 4. The appearance of shear bands at strain rate of 1 s^{-1} and temperatures of: a) 650 °C, b) 700 °C.

In Fig. 5, the temperature distribution of the specimens deformed at the temperature of 650 °C and strain rates of 0.001 s^{-1} and 1 s^{-1}up to strain of 0.7 was predicted using Deform software. It was obviously observed that the temperature gradient is insignificant for the specimen deformed at strain rate of 0.001 s-1. However, the maximum temperature gradient is appeared in the specimen deformed at the strain rate of 1 s^{-1}. By decreasing the strain rate, the temperature gradient is significantly reduced.

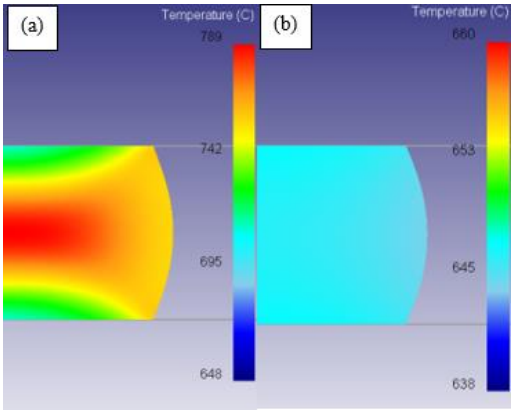

Fig. 5. The temperature gradient distribution of the specimens deformed at 650 °C up to strain of 0.7 and various strain rates of: a) 0.001 s^{-1} and b) 1 s^{-1}.

The strain distribution in the specimens deformed at 800 and 850 °C and strain rate of 0.001 s^{-1} is presented in Fig. 6. As it is seen, despite applying the plastic strain up to 0.7, some regions of the specimen experience much more strains. The main reason for this phenomenon is that in the region between surface of the specimen and die, friction causes high degree of resistance to the deformation. The comparison of the strain distribution contour for the specimens deformed at 800 and 850 °C, revealed that by decreasing the deformation temperature, the value of the effective strain has been noticeably increased. This is attributed to the fact that the workability of the material decreases by reduction of temperature. Therefore, the dead zone region was increased and the value of the strain which is generated in this region is decreased. Consequently, the strain in the center of the specimen is localized.

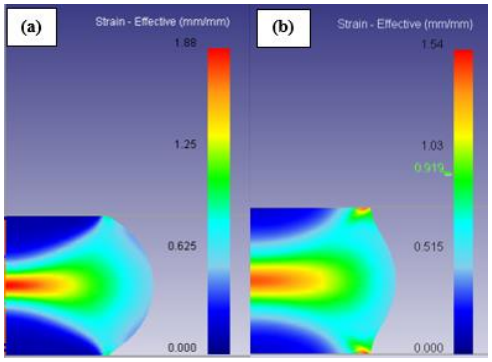

Fig. 6. The strain distribution of the specimens deformed at strain rate of 0.001 s^{-1} and temperatures of: a) 800 °C, and b) 850 °C.

The stress strain curves of the alloy before and after friction and adiabatic heating corrections are shown in Figure 7. It should be noted that the result is only represented for the specimens tested at 650 °C as an example of all test temperatures. As it is seen, by adiabatic heating correction, the uncompensated curves shift to higher values of flow stress confirms the adiabatic heating effect for softening this titanium alloy. Whereas, the flow curves show the inverse behavior after friction correction supports the effect of friction for increasing the force and consequently the stress between specimens and mandrel.

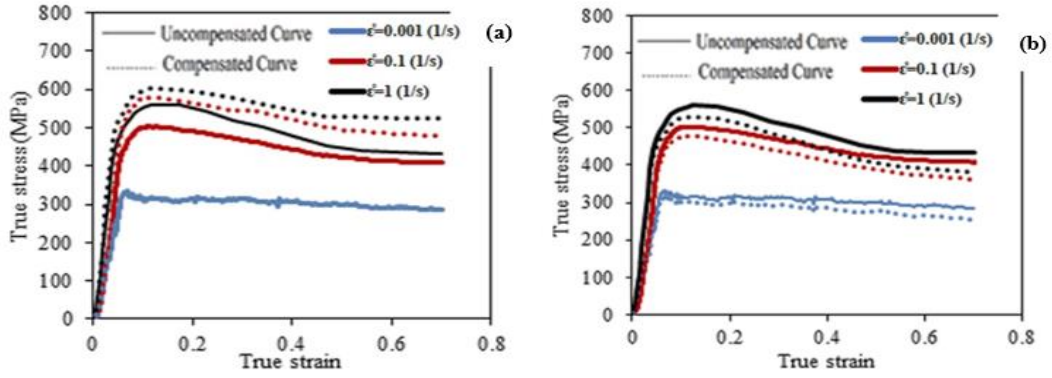

Fig. 7. True stress–true strain curves of the alloy before and after (a) adiabatic heating and (b) friction corrections at the temperature of 650 °C.

The representative friction and adiabatic heating-corrected curves are shown in Figure 8. As it is seen, at all temperatures and strain rates the role of the heat of deformation in comparison with the friction is more. The effect of the flow stress has been influenced by the friction from early stages of the plastic deformation. However, the Adiabatic heating is attributed to the plastic work. Therefore, its value for the early stages of the plastic deformation is insignificant.

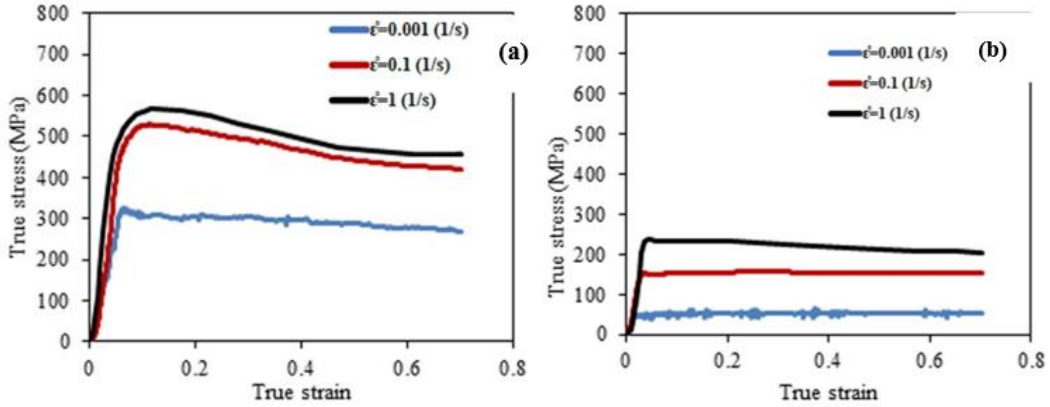

Fig. 8. True stress–true strain curves of the alloy before and after friction and adiabatic heating correction at the temperatures of: a)650 °C, and b)850 °C.

3.2. Microstructural evolution of the Ti-3873 alloy after compression test

The optical micrographs of the alloy after warm deformation at 850 °C and strain rates of the 1, 0.1, and 0.001 s^{-1} are illustrated in Fig. 9. As it is seen in Fig. 9 (a), dynamic recrystallization has occurred to a limited extent. However, the time for occurrence of dynamic restoration processes was insufficient. By decreasing the strain rate (lower value of Z parameter), grain boundary serrations can be observed clearly. Researchers declared [24] that by increasing the deformation temperature and decreasing the strain rate, as a result of dynamic recovery, the grain boundaries migrate locally in response to the boundary tensions of the subgrains and to local dislocation density variations. Consequently, they become serrated with a wavelength which is closely related to their subgrain size. Therefore, dynamic recovery occurred at the temperature of the 850 °C and strain rates of 0.001 and 0.1 s^{-1}.

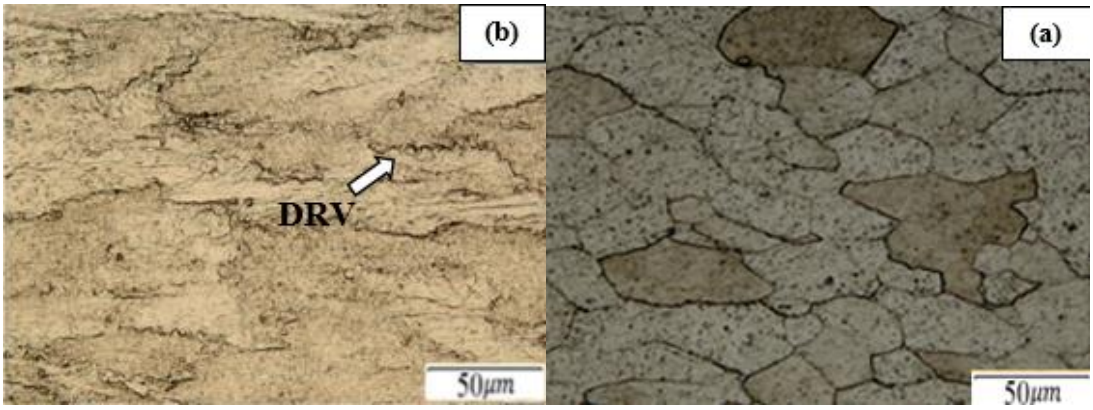

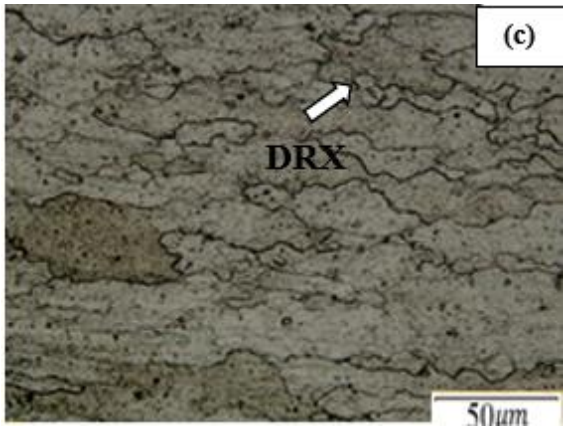

Fig. 9. The microstructure of the specimens deformed at the temperature of 850 °C and strain rates of a) 1, b) 0.1, c)0.001 s^{-1}.

According to the previous studies [18], the dynamic recovery is the dominant softening mechanism via warm working of the β- titanium alloy. However, continuous dynamic recrystallization (CDRX) may be occurred at high strains. The required condition for the occurrence of continuous dynamic recrystallization is the gradual rotation or migration of the sub-grains via recovery process and the transition from low angle grain boundaries (LAGBs) to high angle grain boundaries (HAGBs). In Fig. 9 (c), some serrated grain boundaries have been observed. The wavelength of these serrations is much more than that presented in Fig. 8 (b). Some fine equiaxed grains located adjacent to the serrated high angle grain boundaries confirmed that dynamic recrystallization has been slightly occurred.

3.3. Constitutive equations for corrected flow curves of the Ti-3873 alloy

Constitutive equations have been defined in order to establish the relationship between the flow stress of a material (σ, MPa) and deformation parameters like strain rate ($\dot{\varepsilon}$, s^{-1}) and temperature (T, K) according to the (Z) equation (E.q. 4). By manipulating three hyperbolic, exponential and power law, the relationship has been derived as below [25]:

$$Z = \dot{\varepsilon} \exp\left(\frac{Q}{RT}\right) \quad (4)$$

The common constitutive equation defined for various alloys is sinus-hyperbolic equation (E.q. 5) Where, R, A, α and n are referred to the material's constant. In this equation the value of σ by considering the behavior of the flow curves is corresponding to the peak stress or the steady state flow stress of the material (MPa) [26].

$$Z = \dot{\varepsilon} \exp\left(\frac{Q}{RT}\right) = A\,[\mathrm{Sinh}\,(\alpha\sigma)]^n \quad (5)$$

The slope of the plot of $\ln(\dot{\varepsilon})$ *vs* versus $\ln(\sinh(\alpha\sigma))$ gives the average value of n in the α/β dual phase and β phase region (see Fig. 10 (a)).

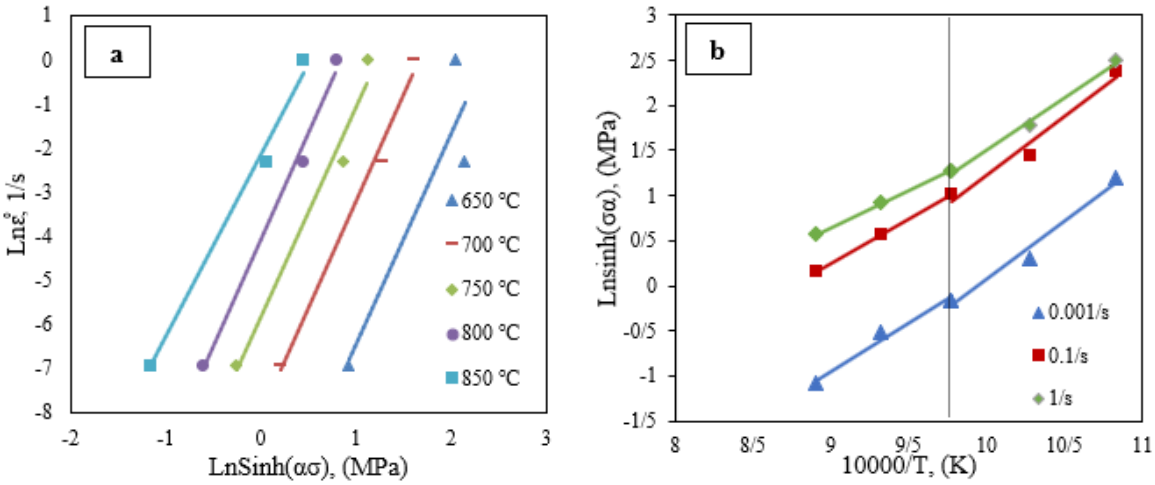

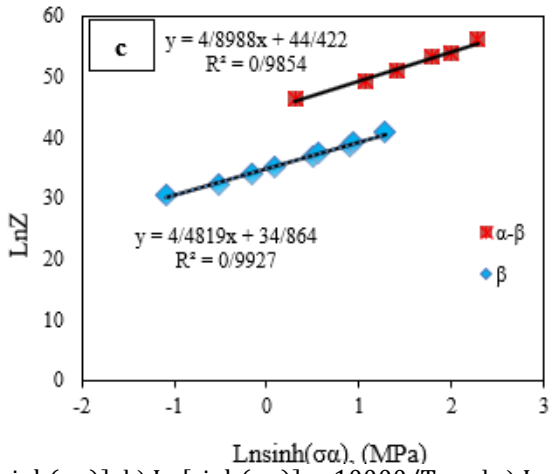

Fig. 10. Plots of a) Ln(ε̇) − Ln[sinh(ασ)], b) Ln[sinh(ασ)] − 10000/T, and c) Ln Z − Ln[sinh(ασ)] at strain of 0.7.

The values of n and α were computed for these regions. It should be mention that for computing these parameters, the specimens were deformed up to strain of 0.7. Then, the value of the s has been determined from the slope of the Ln(sinh(ασ) - 1000/T), (see Fig. 10 (b)). Based on Q=nsR relationship, the activation energy of the warm deformation process was computed. Therefore, the activation energy of the Ti-3873 alloy in the temperature range of 650-850 °C and strain rates of 0.001, 0.1 and 1 s-1 for dual phase α/β and single phase β regions are calculated as 429 and 353 kJ/mol, respectively. As a result of the variation of α parameter in single and dual phase regions and due to the difference in the Q value of these regions, the diagrams illustrated in Fig. 10. (b) and 10. (c) are divided into two distinct regions with different equations. The resultants constitutive equations for warm deformation of the alloy in α/β and β regions are as follows:

$$\dot{\varepsilon} = \exp(44.4)\,.\,[Sinh(0.0065\,\sigma)]^{4.61}.\exp\left(\frac{-429000}{RT}\right)$$

$$\dot{\varepsilon} = \exp(34.8)\,.\,[Sinh(0.0065\,\sigma)]^{4.4}.\exp\left(\frac{-353000}{RT}\right)$$

Jonas et al [27] demonstrated that the variation of Q for dual phase α/β region in comparison to β phase region is related to the difference between the flow stress of the hard α phase and soft β phase. The other important parameter which affects the variation of Q is the dependence of volume fraction of α phase to the temperature.

It has been proved that at low flow stresses (ασ<0.8), Eq. (5) is changed to a power-law equation as below:

$$Z = \dot{\varepsilon}\exp\left(\frac{Q}{RT}\right) = A\sigma^{n} \quad (8)$$

$$\dot{\varepsilon} = A\sigma^{n}\exp\left(-\frac{Q}{RT}\right) \quad (9)$$

where A and n are material constants. In order to determine them, the LnZ vs Lnσ plotted (see Fig. 11).

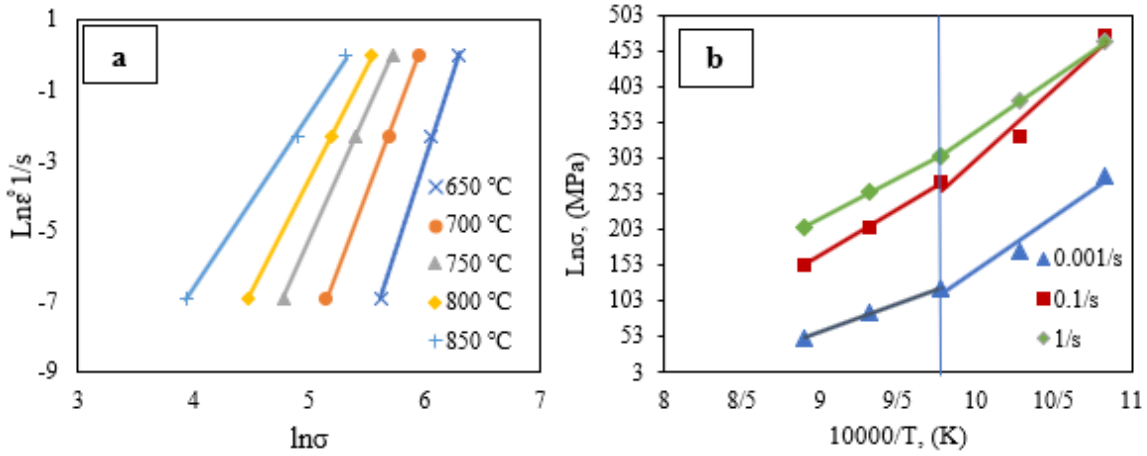

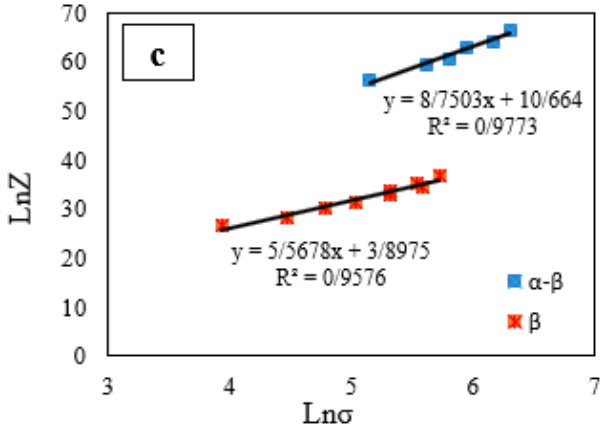

Fig. 11. Plots of (a) $\mathrm{Ln}[\sigma] - \mathrm{Ln}(\dot{\varepsilon})$, b) $\mathrm{Ln}[\sigma] - 10000/\mathrm{T}$, and c) Ln Z $-$ $\mathrm{Ln}[\sigma]$ at strain of 0.7.

As it is seen, the value of n for the dual phase α/β and single phase β is obtained as 9.4 and 6.1, respectively. Moreover, using LnZ vs Lnσ diagram, the value of A for dual phase α/β and single phase β regions is determined as 10.3 and 6.8, respectively. Hence, there is a linear relationship between the stress and Z as given by the following equations (Eq. 10 and Eq. 11) for the dual phase α/β and single phase β regions, respectively:

$$Z = 10.3 \times \sigma^{9.4} \quad (10)$$

$$Z = 6.8 \times \sigma^{6.1} \quad (11)$$

Finally, the power-law relation is given by the following equations (Eq. 12 and Eq. 13) for the dual phase α/β and single phase β regions, respectively:

$$\dot{\varepsilon} = 10.3\sigma^{9.4}\exp\left(\frac{-510000}{RT}\right) \quad (12)$$

$$\dot{\varepsilon} = 6.8\sigma^{6.1}\exp\left(\frac{-314000}{RT}\right) \quad (13)$$

At high flow stresses (ασ>1.2), the Eq. (5) is changed to an exponential form as below: [28, 29]:

$$Z = \dot{\varepsilon}\exp\left(\frac{Q}{RT}\right) = B\exp(\beta\sigma) \quad (14)$$

where, B and β are referring to the constant parameters of the material. This equation, similar to the previous equation, the sigma is referred to the peak stress or the steady state stress (MPa). For the purpose of determining the constant parameters of the exponential equation, the logarithmic form of the equation 14 was derived. Therefore, the equation was correlated in linear form. For obtaining the exponential relationship, the $\mathrm{Ln}(\dot{\varepsilon}) - \mathrm{Ln}(\beta\sigma)$ plots were presented in Fig. 12. According to Fig. 12 (a), the n parameter for dual phase and single phase is obtained as 10.31 and 5.3, respectively.

The S parameter can be determined from the slope of the plot of the σ –10000/T diagram, as shown in Fig. 12 (b), S determined as 0.53 and 0.61 for dual phase α/β and single phase β regions, respectively. The intercept in the plot of $\mathrm{Ln}Z - \beta\sigma$, gives the value of A for both regions.

The modified exponential equation is given by the following equations (Eq. 15 and Eq. 16) for the dual phase α/β and single phase β regions, respectively:

$$\dot{\varepsilon} = 43.91[(0.033\,\sigma)]^{\cdot}.\exp\left(\frac{-453000}{RT}\right) \quad (15)$$

$$\dot{\varepsilon} = 23.5[(0.039\,\sigma)]^{\cdot}.\exp\left(\frac{-268000}{RT}\right) \quad (16)$$

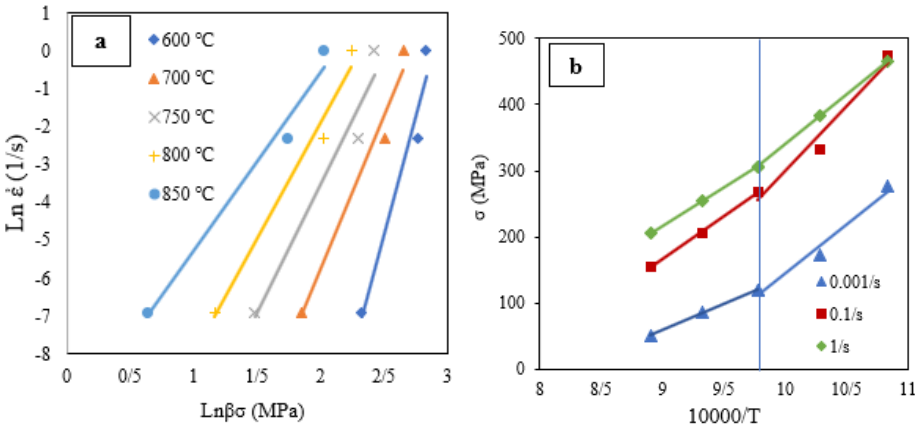

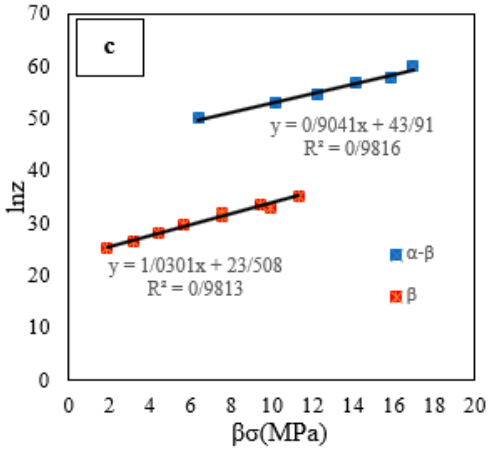

Fig. 12. Plots of a) $Ln(\dot{\varepsilon}) - Ln(\beta\sigma)$, b) $(\sigma) - \frac{10000}{T}$, and c) $LnZ - \beta\sigma$ at strain of 0.7.

From the regression analysis of the relation between the flow stress and Z parameter, the R2 has been computed for each equation as shown in Table 3. As it is seen, the hyperbolic equation represents an acceptable prediction of the experimental flow curves of the Ti-3873 alloy.

Table 3. The derived activation energy (Q), R2, and constitutive equations obtained for the Ti-3873 alloy.

Approach	region	Energy Activation e (kJ/mol)	Constitutive equation	Adj .R-Square
Hyperbolic	α/β	429	$Z = (44.4).[Sinh(0.0065\,\sigma)]^{4.61}$	R2=98.5
	β	353	$Z = (348).[Sinh(0.0065\,\sigma)]^{4.4}$	R2=99.8
Power-law	α/β	510	$Z = 10.3 \times \sigma^{9.4}$	R2=97.7
	β	314	$Z = 6.8 \times \sigma^{6.1}$	R2=95.7
Exponential	α/β	453	$Z = 43.91\exp[(0.033\,\sigma)]$	R2=98.1
	β	268	$Z = 23.5\exp[(0.039\,\sigma)]$	R2=98.1

The activation energy for hot deformation of some titanium alloys is summarized in Table 4. It has been reported that [29] the predominant restoration mechanism during hot deformation of β-titanium alloys at low Zener-Holloman range is dynamic recovery. Therefore, the deformation of β-titanium in single β phase region is accompanied with the formation and development of substructure. In this research, at the temperature of 850 °C and strain rate of 0.001 s^{-1}, a plateau form of flow curve and the serrated grain boundaries with a few recrystallized grains in the microstructure of the Ti-3873 alloy, represents dynamic recovery behavior. The high activation energy for deformation of the Ti-3873 alloy in single β phase region is attributed to dynamic recovery and extended dynamic recrystallization. Similar behavior was also reported for the IMI-834 and Ti-6Al-4V alloys in which dynamic recovery and consequently dynamic recrystallization occurred during deformation them in single phase β region [30, 31].

Table 4. The activation energy for hot deformation of some titanium alloys [26].

alloy	Initial microstructure	Activation energy (kJ/mol)	
		Single phase β	Dual phase α/β
SP-700	Plate-like α phase	305.5	165.2
Ti-6Al-4V	Equiaxed α phase	530	376
Ti–5Al–5Mo–5V–3Cr–1Zr	Globular α phase	148	275

The main reason for the higher value of the activation energy at dual phase α/β region is the occurrence of the dynamic globularization [26]. In Fig. 13, the SEM microstructure of the specimens deformed at the temperature of 650 and 700 °C and strain rate of 0.001 is exhibited. Both images show the dual phase α/β microstructure. The difference between these two images is the morphology of the phases. As it is seen, the microstructure of the specimen deformed at 650 °C includes lamellar and globular α phase in the β matrix. However, by increasing the temperature to 700 °C, the globularization of α phase has been accomplished. Therefore, dynamic globularization of α phase may cause higher activation energy during deformation of the Ti-3873 alloy.

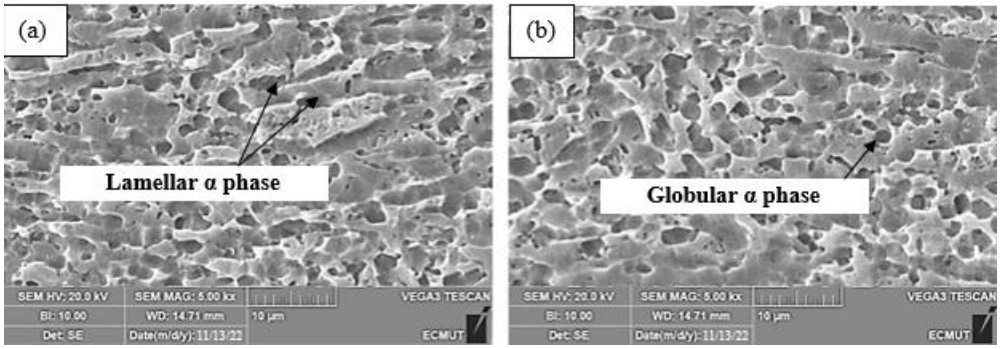

Fig. 13. The SEM images of the specimens deformed at: a) 650 °C and b) 700 °C and strain rate of 0.001 s^{-1}.

3.4. Prediction of workability of the alloy using processing map

Processing maps have been provided according to the dynamic model of the materials. It was assumed that the energy has been consumed via deformation process of the material. The content of the energy loss for the specified condition of the deformation has been defined based on the variation of the stress versus variation of the strain rate. This parameter ($m = \frac{\partial \operatorname{Ln} \sigma}{\partial \operatorname{Ln} \dot{\varepsilon}}$) is referred to the strain rate sensitivity coefficient. It is obvious that the major part of the energy loss is converted to the heat of the deformation resulted in increasing the temperature of the material via plastic deformation. While a very minor part of the energy loss leads to the evolution of microstructure. The power dissipation efficiency (η) of the material is defined as [32]:

$$\eta(T, \dot{\varepsilon}) = \frac{2m}{m+1} \quad (17)$$

Therefore, η is the parameter determining the extent of power dissipation as a consequence of microstructural evolution. In most cases, the maximum value of η corresponds to the optimum deformation condition of the alloy. Although in some conditions high value of η is a result of super plasticity or crack formation. The variation of η with temperature and strain rate represents the characteristics of power dissipation through microstructural evolution constitutes a power dissipation map of the Ti-3873 alloy.

A continuum instability criterion [33] developed on the basis of extremum principles of irreversible thermodynamics, is used to delineate the regimes of flow instability. This criterion is given as:

$$\xi(\dot{\varepsilon}) = \frac{\partial\, Ln[m/(m+1)]}{\partial\, Ln\, \dot{\varepsilon}} + m < 0 \quad (18)$$

The instability parameter, $\xi(\dot{\varepsilon})$, is evaluated as a function of temperature and strain rate and plotted to obtain an instability map of the alloy. This map should be superimposed on to the power dissipation map to obtain a processing map of the alloy. The processing map of the Ti-3873 alloy obtained at a strain of 0.7 is shown in Fig. 14. As it is seen, the efficiency value intensified by increasing the temperature and decreasing the strain rate; and vice versa. The processing map of the alloy can be divided to three regions.

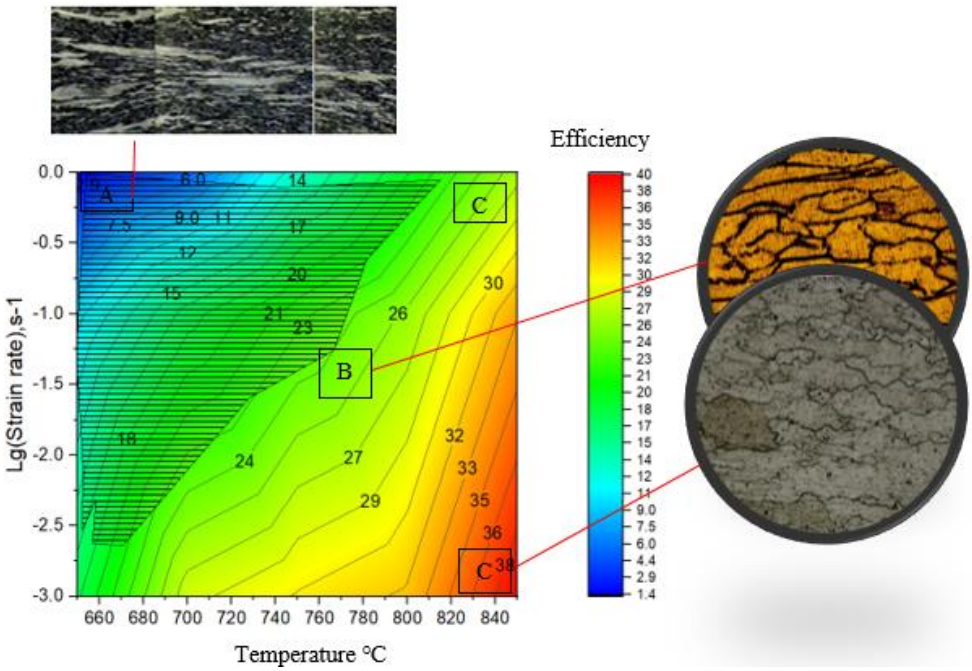

Fig. 14. The processing map of the Ti-3873 alloy deformed at strain of 0.7.

Region A: The temperature range of 650 to700 °C and strain rates of 0.1 and 1 s^{-1} with the efficiency lower than 25 %. This region related to the domain where the deformation was in the dual phase α/β region. The bands appeared in the structure of the deformed specimens presented in Fig. 4 clearly reveal their direction with the applied stress which is between 30 to 45%. The heat of deformation is remained undissipated because of lower thermal conductivity of titanium alloys, leading to a considerable rise in the temperature of the specimen due to inadequate time interval. Therefore, this localization is due to flow softening as a result of adiabatic heating during deformation at high Z values. Consequently, if the localization becomes more severe; the cracks will be formed along the shear bands.

Region B: The temperature range of 720 to 800 °C and strain rates of the 0.001, 0.1 and 1 $s^{-1}$where the efficiency is slightly in the range of 25-32 %. This region belongs to deformation at single phase β region.

Zone C: The temperature range of 800-850 °C and strain rate of 0.01 and 0.001 s^{-1} where the peak efficiency of 39 % is observed. This region is located in the single phase β region where deformation occurred at low values of Z parameter. Regrading to Fig. 9 (a), the appearance of serrated grain boundaries and new grains suggests that the dissipative mechanism like dynamic recovery is the predominant mechanism. Therefore, it can be concluded that the optimum condition for thermomechanical processing of the Ti-3873 alloy is at temperature range of 800-850 °C and strain rate of 0.1 and 0.001 s^{-1}.

4. Conclusion

The flow curves at high strain rate of 1 s^{-1} and low temperatures of 650 and 700 °C employed corrections for adiabatic heating and friction showed a peak stress followed by softening to a steady state one.

The flow curves at low strain rate of 0.001 s^{-1} and high temperatures of 800 and 850 °C corrected for adiabatic heating and friction showed a steady state behavior in which the stress remained essentially constant from initial yielding to the maximum strain. Constitutive equations formulated to describe the temperature dependence of the flow stress over a wide range of strain rate indicate an apparent activation energy of 429 and 353 kJ mol^{-1} for deformation at dual phase α/β and single phase β regions, respectively.

Three distinct regions of deformation have been observed in the processing map: at temperature range of 650 to700 °C and strain rates of 0.1 and 1 s^{-1} with the efficiency lower than 25 %, wherein the adiabatic shear bands are formed; at the temperature range of 720 to 800 °C and strain rates of the 0.001, 0.1 and 1 $s^{-1}$where the efficiency is slightly in the range of 25-32 %; and the temperature range of 800-850 °C and strain rate of 0.01 and 0.001 s^{-1} where the peak efficiency of 39 % was obtained.

The preferable regions for hot workability of the Ti-3873 alloy were achieved at the temperature range of 800-850 °C and strain rate of 0.1 and 0.001 s^{-1} where the alloy undergoes dynamic recovery and consequently dynamic recrystallization which is attributed to the appearance of serrated grain boundaries and few recrystallized grains.

References

[1] M. Abdel-Hady, K. Hinoshita and M. Morinaga "General approach to phase stability and elastic properties of β-type Ti-alloys using electronic parameters", Scr. Mater., Vol. 55, 2006, pp. 477–480.

[2] P. Lacombe, The 6th World Conference on Titanium. Cannes Paris. Les Edition de Physics. Part 4, 1989

[3] D. Kuroda, M. Niinomi, M. Morinaga, Y. Kato and T. Yashiro "Design and mechanical properties of new β type titanium alloys for implant materials", Mat. Sci. Eng. A, Vol. 243, 1998, pp. 244–24.

[4] S. Sadeghpour, S. M. Abbasi, M. Morakabati, L. P. Karjalainen and D. A. Porter "Effect of cold rolling and subsequent annealing on grain refinement of a beta titanium alloy showing stress-induced martensitic transformation" Mat. Sci. Eng. A, Vol. 731, 2018, pp. 465–478.

[5] S. Sadeghpour, S. M. Abbasi, M. Morakabati, A. L. P. Kisko, Karjalainen and D. A. Porter, "On the compressive deformation behavior of new beta titanium alloys designed by d-electron method", J. All. Comp., Vol. 746, 2018, pp. 206–217.

[6] F. S. Froes, "Titanium for medical and dental applications-An introduction. In Titanium in medical and dental applications. Australia. Elsevier. 2018

[7] S. Sadeghpour, S. M. Abbasi and M. Morakabati "Deformation-induced martensitic transformation in a new metastable β titanium alloy" J. All. Comp., Vol. 650, 2015, pp. 22–29.

[8] P. Laheurte, F. Prima, A. Eberhardt, T. Gloriant, M. Wary and E. Patoor "Mechanical properties of low modulus β titanium alloys designed from the electronic approach", J. Mech. Beh. Bio. Mat. 3, 2010, pp. 565–573.

[9] F. Sun, J. Y. Zhang, M. Marteleur, C. Brozek, E. F. Rauch, M. Veron and F. Prima, A new titanium alloy with a combination of high strength, high strain hardening and improved ductility, Scr. Mater., Vol. 94, 2015, 17-2.

[10] F. Chen, G. Xu, X. Zhang and K. Zhou, "Exploring the phase transformation in β-quenched Ti-5553 alloy during continuous heating via dilatometric measurement, microstructure characterization, and diffusion analysis", Metall. Mat. Trans. A, 2016, Vol. 47, pp. 5383–539.

[11] Y. Q. Jiang, Y. C. Lin, X. Y. Zhang, C. Chen, Q. W. Wang and G. D. Pang "Isothermal tensile deformation behaviors and fracture mechanism of Ti-5Al-5Mo-5V-1Cr-1Fe alloy in β phase field", Vacu., Vol 156, 2018, pp. 187-197.

[12] V. N. Moiseev,"Beta-titanium alloys and prospects of their development", Metal. Sci. Heat Treat., Vol. 40, 1998, pp. 482-485.

[13] G. Lütjering and J. C. Williams, "Titanium", 2007, Germany, Springer, p. 125.

[14] S. Sadeghpour, S. M. Abbasi, M. Morakabati and L. Karjalainen, "Effect of dislocation channeling and kink band formation on enhanced tensile properties of a new beta Ti alloy", J. Alloy. Comp., Vol. 808, 2019, 151741.

[15] S. M. Abbasi, M. Morakabati, A. H. Sheikhali and A. Momeni," Hot deformation behavior of beta titanium Ti-13V-11Cr-3Al alloy", Metall. Mate. Trans. A, Vol. 45, 2014, pp. 5201–5211.

[16] Y. C. Lin, J. Huang, H. B. Li and D. D. Chen, "Phase transformation and constitutive models of a hot compressed TC18 titanium alloy in the α+ β regime", Vacuu., Vol 157, 2018, pp. 83-91.

[17] S. M. Abbasi, A. Momeni, Y. C. Lin and H. R. Jafarian, "Dynamic softening mechanism in Ti-13V-11Cr-3Al beta Ti alloy during hot compressive deformation", Mat. Sci. Eng. A, Vol. 665, 2016, 154–160.

[18] A. Momeni, S. M. Abbasi and S. Sadeghpour, "Comparative study on the hot deformation behavior of Ti-5Al-5Mo-5V-3Cr and newly developed Ti-4Al-7Mo-3V-3Cr alloys", J. Vacuu. Vol. 161, 2019, pp. 410-418.

[19] X. Ma, W. Zeng, B. Xu, Y. Sun, C. Xue and Y. Han, "Characterization of the hot deformation behavior of a Ti–22Al–25Nb alloy using processing maps based on the Murty criterion", Interme, Vol. 20(1). 2012, pp. 1-7.

[20] Y. Zhu, W. Zeng, F. Feng and Y. Sun "Characterization of hot deformation behavior of as-cast TC21 titanium alloy using processing map" Mat. Sci. Eng. A, Vol. 528(3), 2011, pp. 1757-1763.

[21] G. E. Dieter, H. A. Kuhn and S. L. Semiatin, "Handbook of workability and process design", 2003ASM international, p. 214.

[22] M. Morakabati, H. Saki, R. Mahdavih, "effect of single-step and two-step aging on the microstructure and mechanical properties of the novel Ti-3Al-8Mo-7V-3Cr alloy", Modares Mech. Eng., 3, Vol. 23, 2023, pp. 199-208.

[23] R. L. Goetz and S. L. Semiatin, "The adiabatic correction factor for deformation heating during the uniaxial compression test" J. Mat. Eng. Perf., Vo. 10, 2001, pp. 710-717.

[24] Y. Han, W. Zeng, Y. Qi and Y. Zhao, "The influence of thermomechanical processing on microstructural evolution of Ti600 titanium alloy", Mat. Sci. Eng. A, Vol. 528, 2011, pp. 8410-8416.

[25] F. J. Humphreys and M. Hatherly, "Recrystallization and related annealing phenomena", Elsevier 2012, p. 251.

[26] A. H. Sheikhali, M. Morakabati and S. M. Abbasi, "Constitutive modeling for hot working behavior of SP-700 titanium alloy", J. Mat. Eng. Perf., Mat. Sci. Eng. A, Vol. 28, 2019, pp. 6525-6537.

[27] J. J. Jonas, C. Aranas, A. Fall and M. Jahazi, "Transformation Softening in Three Titanium Alloys", Mat. Des., Vol. 113, 2017, pp. 305- 310.
[28] K. Q. Lv, W. H. Cai, Z. Li, Z. Sh. Nong, L. Zhang, "Study on the Microstructure and Mechanical Properties of Dynamic Recrystallization of Metastable β Titanium Alloy", Materials Science Forum, Vol. 1064, 2022, pp. 177-182.
[29] A Esmaeilpour, HR Abedi, A Mirzaei, A Habibiyan, "Constructing the high temperature efficiency and instability maps of selective laser melted 316L stainless steel through artificial neural network modeling", J. Mat. Res. Tech., 2022, Vol. 18, pp. 4578-4589.
[30] P. Wanjara, M. Jahazi, H. Monajati and S. Yue, "Influence of thermomechanical processing on microstructural evolution in near-α alloy IMI834" Mat. Sci. Eng. A, Vol. 416, 2006, pp. 300-331.
[31] A. Momeni and S. M. Abbasi, "Effect of hot working on flow behavior of Ti-6Al-4V alloy in single phase and two phases regions", Mat. Des., Vol. 31, 2010, pp. 3599-3604.
[32] Y. V. R. K. Prasad, K. P. Rao and S. Sasidhar, "Hot working guide a compendium of processing maps", 2015, ASM international, p. 156.
[33] Y. P. Li, H. Matsumoto and A. Chiba, "Correcting the Stress-Strain Curve in the Stroke-Rate Controlling Forging Process" Metall. Mat. Trans. A, Vol. 40, 2009, pp. 1203-1211.